

Effects of 5-(3-Aminophenyl)-tetrazole as a Corrosion Inhibitor on the Corrosion of Mg/Mn alloy in Arabian Gulf Water

El-Sayed M. Sherif^{1,*}

¹ Center of Excellence for Research in Engineering Materials (CEREM), College of Engineering, King Saud University, P. O. Box 800, Al-Riyadh 11421, Saudi Arabia

*E-mail: esherif@ksu.edu.sa

Received: 12 September 2011 / Accepted: 5 October 2011 / Published: 1 November 2011

The effects of 5-(3-aminophenyl)-tetrazole (APT) as a corrosion inhibitor for Mg-Mn alloy after its immersion in naturally aerated stagnant Arabian Gulf water (AGW) for 1 h and 150 h have been reported. The study has been carried out using a combination of electrochemical and gravimetric measurements along with scanning electron microscope (SEM) and X-ray energy dispersive (EDX) investigations. Electrochemical measurements showed that the corrosion of Mg-Mn alloy in AGW decreases with increasing exposure time as well as in the presence of APT and the increase of its concentration. Weight-loss tests after varied exposure intervals proved that the corrosion rate of the alloy decreases with increasing time and APT content. The SEM and EDX investigations revealed that APT molecules inhibit the corrosion of Mg through repairing the weak areas on its surface, which leads to increasing the corrosion resistance for the alloy against the corrosive attack of AGW.

Keywords: Arabian Gulf water; Mg-Mn alloy; corrosion inhibition; 5-(3-aminophenyl)-tetrazole

1. INTRODUCTION

Magnesium alloys have been widely used in so many applications because of their low density, good heat dissipation, good damping, and good electro-magnetic shield [1-6]. Magnesium alloys usually form an oxide layer on their surfaces. This layer does not protect the alloy from being corroded, especially in chloride containing environments. This occurs because the Cl⁻ ions penetrate the oxide layer reaching the surface to react with the metal substrate. The high corrosion susceptibility is also expected as a result of the high active potential of Mg. Furthermore, the presence of impurities and second phases within the alloy act as cathodic sites that accelerate the local galvanic corrosion of

the alloy matrix [7]. Therefore, controlling the corrosion of Mg alloys in corrosive media has been attracted numerous investigators [8-12].

Protection of metals and alloys against corrosion in harsh environments using corrosion inhibitors has been largely reported [13–21]. Several researchers have been devoted to the protection of magnesium but very little work has been seldom involved on the adding corrosion inhibitors [14]. The inhibition of magnesium engine block in commercial coolants by KF has been reported [20]. Alkyl carboxylate was used to inhibit the corrosion of magnesium in sodium decanoate solutions as a result of the hydrophobic features of the aliphatic chains in its structure [22]. Other compounds such as sodium dodecylsulphate, phytic acid, ethylenediamine tetraacetic acid, p-nitro-benzene-azo-resorcinol, acidum tannicum or stearic acid were used at a concentration of 5.0 mM to inhibit the corrosion of AZ61 magnesium alloy in alkali aqueous solution [23]. These compounds have the ability to form an inhibitor-magnesium precipitation in aqueous solution. The formation of such precipitation effectively inhibits the increase of polarization current density as well as the dissolution and oxidation of magnesium alloys [23].

In the present work, the corrosion of Mg-Mn alloy in naturally aerated AGW after different exposure intervals and its inhibition by APT were investigated. The chemical structure of APT (as seen in Fig. 1) shows that it is a heterocyclic compound containing a variety of donor atoms. The presence of such atoms is expected to increase the adsorption susceptibility of APT molecules onto Mg surface protecting it from being attacked by AGW. It is worth to mention that APT has been reported to act as a good corrosion inhibitor for copper [19, 24], iron [25] and Mg [26] in chloride media. Our study has been carried out using cyclic potentiodynamic polarization, current-time at constant potential, electrochemical impedance spectroscopy and weight-loss measurements along with SEM and EDX investigations.

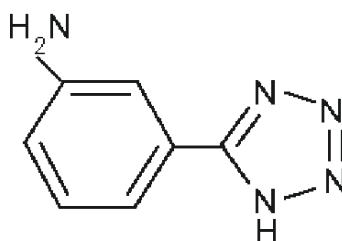


Figure 1. Chemical formula of 5-(3-aminophenyl)-tetrazole (APT)

2. EXPERIMENTAL

2.1. Chemicals, electrochemical cell, and electrochemical techniques

Natural Arabian Gulf water (AGW) was obtained from the Arabian Gulf at the eastern region (Dammam, Kingdom of Saudi Arabia), 5-(3-Aminophenyl)-tetrazole (APT, Alfa-Aesar, 96%), and absolute ethanol (C_2H_5OH , Merck, 99.9%) were used as received. An electrochemical cell with a

three-electrode configuration was used; a Mg-07%Mn rod having 1.2 cm side length and total surface of 1.44 cm², a platinum foil, and an Ag/AgCl electrode (in a saturated KCl) were used as the working, counter, and reference electrodes, respectively.

Electrochemical experiments were performed by using an Autolab Potentiostat (PGSTAT20 computer controlled) operated by the general purpose electrochemical software (GPES) version 4.9. The polarization curves were obtained by scanning the potential in the forward direction from -2000 to -800 mV against Ag/AgCl at a scan rate of 3.0mV/s; the potential was then reversed in the backward direction at the same scan rate. Current-time measurements at constant anodic potential were carried out by stepping the potential of the magnesium rods to -1200 mV versus Ag/AgCl. Electrochemical impedance spectroscopy data were obtained at open circuit potential over a frequency range from 100000 Hz to 0.1Hz, with an ac wave of ± 5 mV peak-to-peak overlaid on a dc bias potential, and the impedance spectra were collected using Powersine software at a rate of 10 points per decade change in frequency. All electrochemical experiments were performed at room temperature in naturally aerated solutions and the data were collected after Mg immersion for 1 h and 150 h.

2.2. Gravimetric measurements

The weight-loss experiments were carried out using rectangular Mg-Mn coupons having a dimension of 4.0 cm length, 2.0 cm width and 0.4 cm thickness. The coupons were polished and dried as for the case of Mg rods, weighed, and then suspended in 300 cm³ solutions of AGW in the absence and the presence of 1.0 mM and 5.0 M APT for varied exposure periods from 5 to 25 days. The values of the loss in weight per area (ΔW), the corrosion rate (K_{Corr}), and the percentage of the inhibition efficiency ($IE\%$) for Mg coupons in the test solutions were calculated as reported in our previous studies [13, 27].

2.3. SEM investigation and EDX analysis

The SEM investigation and EDX analysis were obtained for the surface of magnesium specimens after their immersions in AGW in absence and presence APT. The SEM micrographs and EDX profile spectra were collected by using a JEOL model JSM-6610LV (Japanese made) scanning electron microscope having an energy dispersive X-ray analyzer attached.

3. RESULTS AND DISCUSSION

3.1. Cyclic potentiodynamic polarization (CPP) measurements

Fig. 2 shows the CPP curves for Mg electrode after its immersion in naturally aerated AGW containing 0.0 mM APT (1), 1.0 mM APT (2) and 5.0 mM APT (3) for 1 h (a) and 150 h (b), respectively. The values of corrosion potential (E_{Corr}), corrosion current density (j_{Corr}), cathodic (β_c) and anodic (β_a) Tafel slopes, protection potential (E_{Prot}), polarization resistance (R_p), and corrosion rate

(K_{Corr}) obtained from CPP curves in addition to the values of the inhibition efficiency ($IE\%$) are listed in Table 1. E_{Corr} and j_{Corr} values were obtained from the extrapolation of anodic and cathodic Tafel lines located next to the linearized current regions. E_{Prot} values were determined from the backward anodic polarization curve at the intersection point with the forward polarization curve. The values of R_p , K_{Corr} and $IE\%$ were calculated from the CPP curves as in our previous work [28–32].

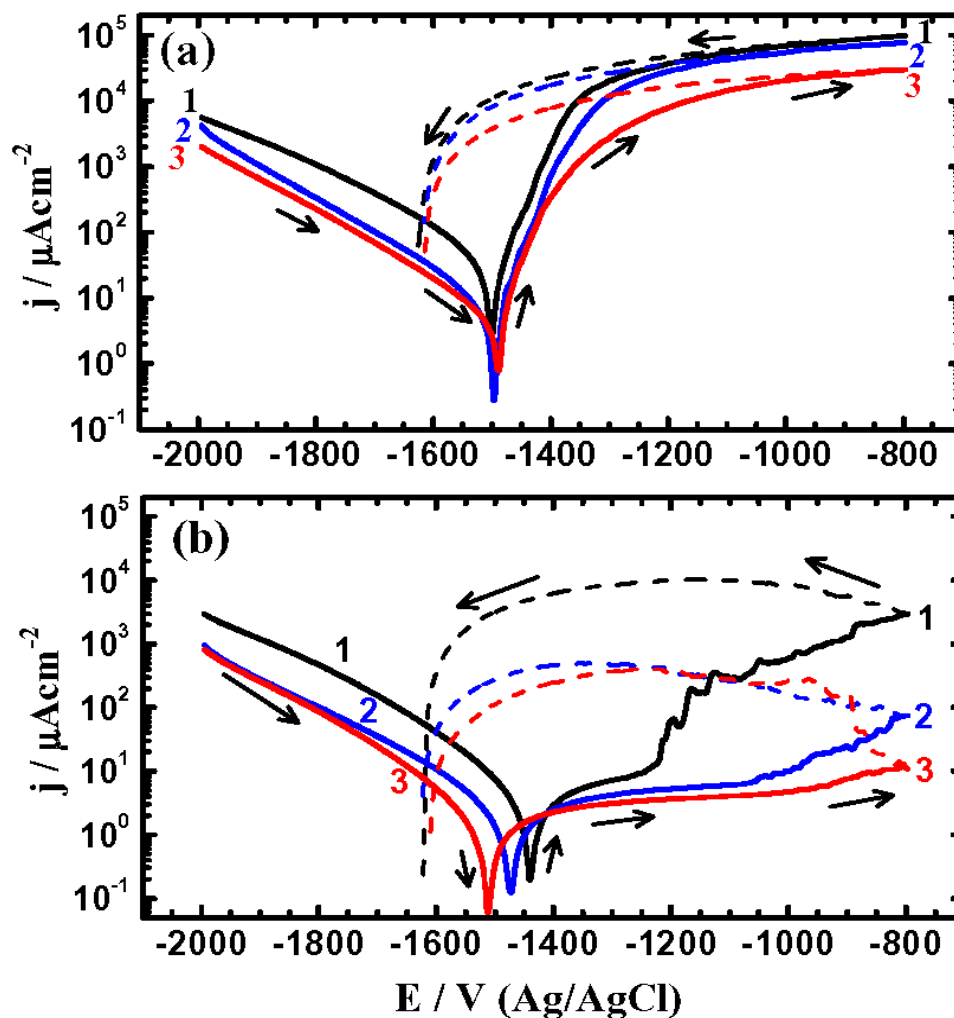


Figure 2. Cyclic potentiodynamic polarization curves for Mg electrode after its immersion in naturally aerated AGW in the absence (1), presence of 1.0 mM APT (2) and 5.0 mM APT for 1 h (a) and 150 h (b), respectively.

The CPP curve 1 (Fig. 2a) shows that an active dissolution occurred for Mg alloy with increasing potential in the anodic side. Further increases in the current were recorded on reversing the direction of potential scan and a large hysteresis loop is observed. The alloy hence suffers severe pitting corrosion. Increasing the immersion time to 150 h (Fig. 2b, curve 1) highly decreased the values of cathodic, j_{Corr} and anodic currents and K_{Corr} , shifted E_{Corr} and E_{Prot} to the less negative direction, and increased R_p and the area of the hysteresis loop (see also Table 1). This indicates that prolonging the

exposure time decreases the uniform dissolution and increases the pitting corrosion of the Mg alloy in AGW. Here, the anodic dissolution of Mg occurs once the metal is in contact with the test electrolyte as follows [33];



The produced magnesium cations react with hydroxide ions presented in the solution due to the dissociation of water according to the reaction;



Pardo et al. [34] have found that the main corrosion product formed on the Mg surface after 10 days immersion in 3.5% NaCl was $\text{Mg}(\text{OH})_2$, which can be formed as follows;



Table 1. Corrosion parameters obtained from cyclic potentiodynamic polarization curves shown in Fig. 2 for the Mg electrode in naturally aerated AGW without and with APT.

Solution	Parameter							
	$E_{\text{Corr}} / \text{mV}$	$j_{\text{Corr}} / \mu\text{A cm}^{-2}$	$\beta_{\text{c}} / \text{mV dec}^{-1}$	$\beta_{\text{a}} / \text{mV dec}^{-1}$	$E_{\text{Prot}} / \text{mV}$	$R_{\text{p}} / \Omega \text{ cm}^2$	$K_{\text{Corr}} / \text{mmy}^{-1}$	IE / %
AGW alone (1 h)	-1504	51.0	225	65	-1620	430	1.165	—
+ 1.0 mM APT (1 h)	-1528	13.0	180	68	-1615	1651	0.297	74.51
+ 5.0 mM APT (1 h)	-1520	7.50	180	70	-1610	2922	0.171	85.32
AGW alone (150 h)	-1420	3.85	138	140	-1617	863	0.088	—
+ 1.0 mM APT (150 h)	-1450	0.90	143	155	-1615	3593	0.022	75.00
+ 5.0 mM APT (150 h)	-1505	0.60	105	150	-1600	4623	0.013	85.27

It is seen from Fig. 2 and Table 1 that the cathodic, j_{Corr} anodic currents and K_{Corr} significantly decreased in the presence of APT and upon the increase of its concentration due to the increased corrosion resistance of Mg in AGW. Also, the values of E_{Corr} shifted to the more negative values, while E_{Prot} slightly moved towards the positive direction, which resulted from the decrease of Mg uniform and pitting corrosion. The slight negative shift in the values of E_{Corr} in the presence of APT is apparently due to decreasing the rate of the cathodic reaction, which can be represented as follows [35];



The source of the hydrogen ions is the dissociated water, as represented by reaction (4). This effect also increased R_p and $IE\%$ values and decreased the area of the hysteresis loop as a result of decreases both uniform and pitting corrosion of Mg in AGW.

3.2. Current–time (CT) measurements, SEM and EDX investigations

The CT measurements were carried out in order to shed more light on the uniform and pitting corrosion of Mg after varied exposure periods in the stagnant AGW at -1200 mV vs. Ag/AgCl. This potential value was determined from polarization curves.

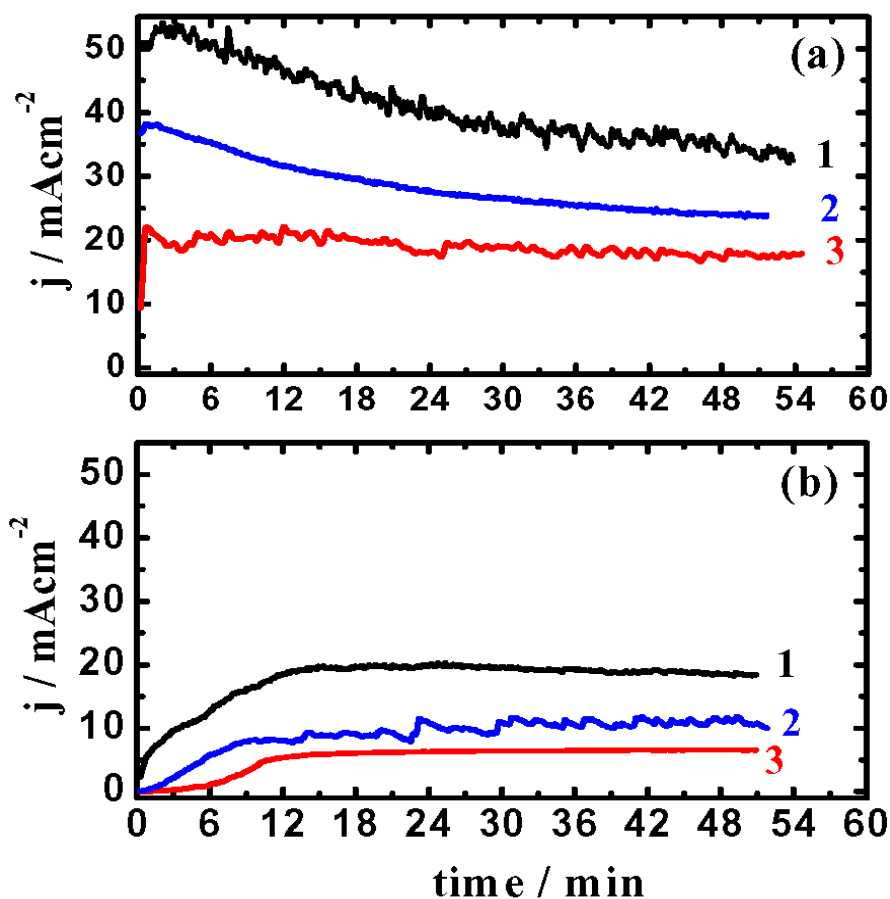


Figure 3. Variations of current versus time at -1200 mV (Ag/AgCl) for Mg electrode after its immersion in naturally aerated AGW in the absence (1), presence of 1.0 mM APT (2) and 5.0 mM APT for 1 h (a) and 150 h (b), respectively.

The variation of the anodic dissolution currents versus time for Mg electrode that was immersed in the naturally aerated AGW in absence (1) and presence of 1.0 mM APT (2) and 5.0 mM APT (3) for 1 h (a) and 150 h (b), respectively before stepping the potential to -1200 mV vs. Ag/AgCl are shown in Fig. 3. The highest current values were recorded for Mg after 1 h immersion in AGW without APT present, Fig. 3a (curve 1). Here, the current showed a rapid increase in the first 3 min due

to the dissolution of an oxide film was formed on the surface of the Mg alloy during its immersion in AGW. The current then slowly decreased accompanied by small fluctuations up to the end of the run. This indicates that the surface developed a large number of initiated small pits [36, 37]. The majority of these pits didn't propagate with time due to the formation of $\text{Mg}(\text{OH})_2$ (eq. 3) that blocked the pits and partially protected the surface from further dissolution for which the absolute current of Mg was decreasing with time. Increasing the immersion time to 150 h (Fig. 3b, curve 1) led to decreasing the initial current values to a minimum. This was related to the formation of a passive film and/or corrosion products, which got thicker with time and partially protected the Mg surface against uniform corrosion. The current then gradually increased in circa the first 25 min due to the occurrence of pitting corrosion. The current stayed almost constant for the rest of the run as a result of the equilibrium between the propagation and blocking of the formed pits. At this condition, the pits develop at sites where oxygen adsorbed on the alloy surface is displaced by an aggressive species such as Cl^- ions that already present in AGW. This is because Cl^- ions have small diameters allows it to penetrate through the oxide film and displace oxygen at the sites where metal-oxygen bond is the weakest [37].

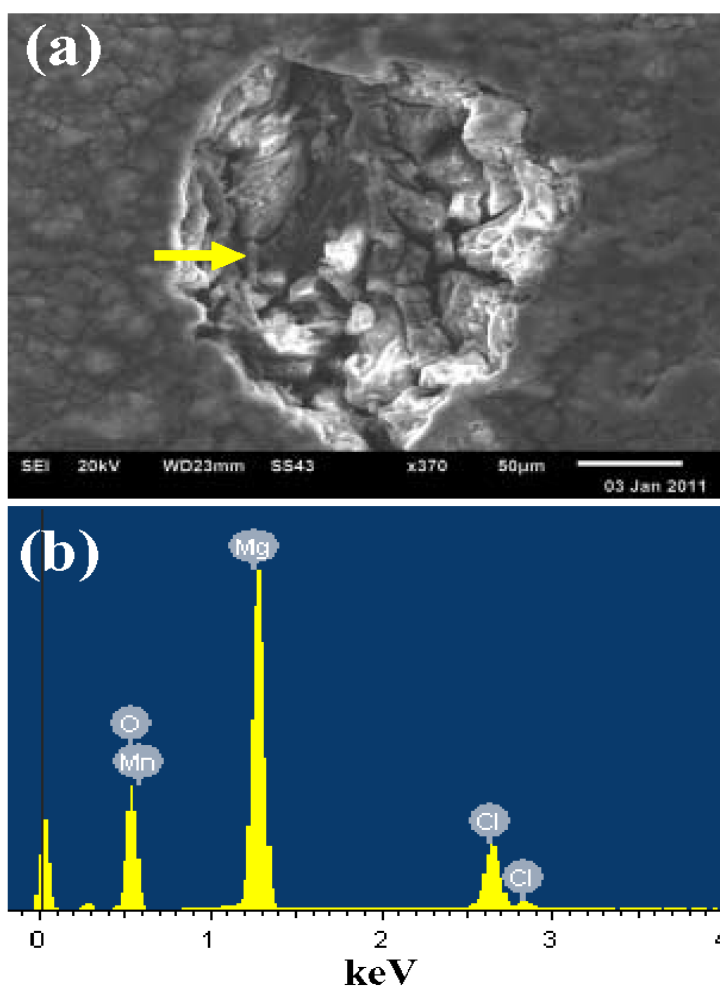


Figure 4. (a) SEM micrograph and (b) the corresponding EDX profile analysis for Mg surface after its immersion in AGW for 150 h followed by stepping the potential to -1200 mV for 1 h.

The addition of 1.0 mM APT to AGW (Fig. 3a, curve 2) decreased both the absolute current and its fluctuations due to the increase of surface compactness by APT molecules. This effect increased with increasing the immersion time to 150 h (Fig. 3b, curve 2), where the APT molecules incorporated within the oxide film and/or corrosion products on Mg. Further increasing of APT concentration to 5.0 mM decreased the absolute current and provided no current fluctuations. This indicates that the presence of APT and the increase of its concentration decreased the Mg uniform and pitting corrosion in the chloride test solution.

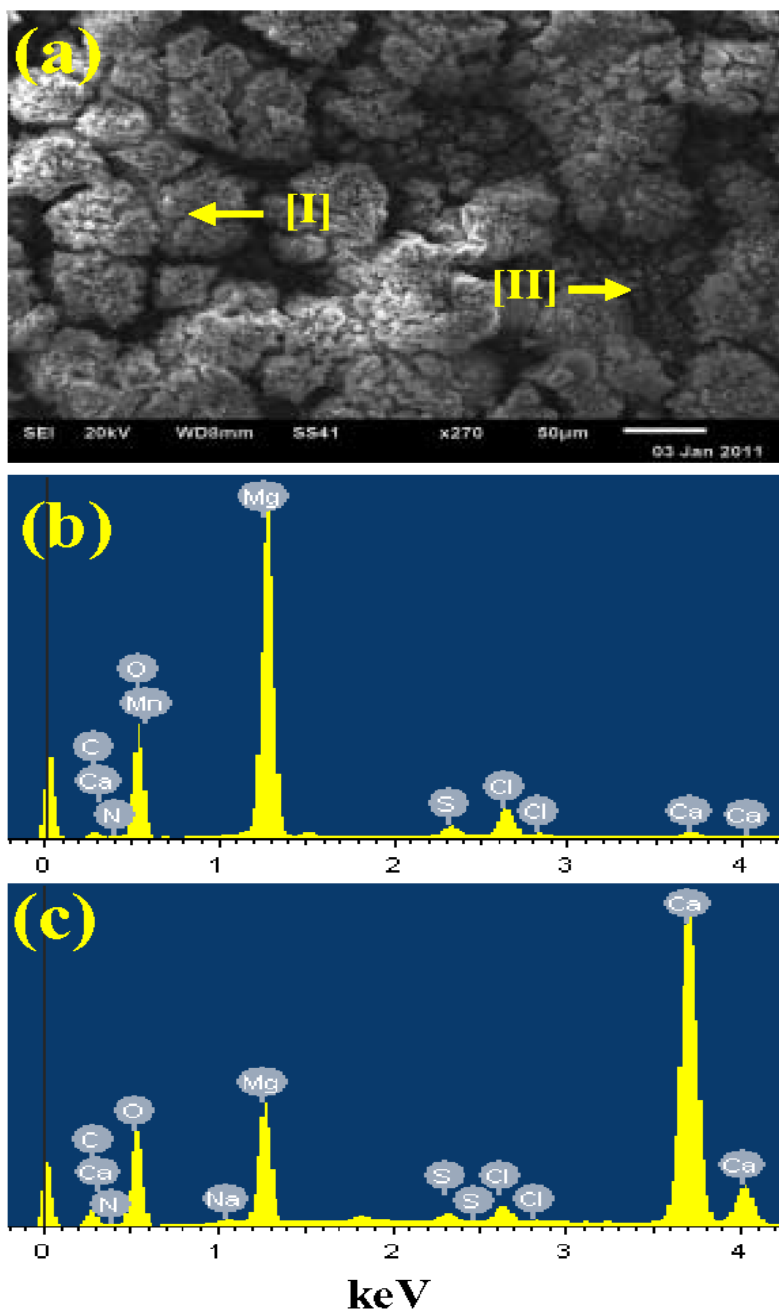


Figure 5. (a) SEM micrograph of Mg surface after its immersion in AGW + 1.0 mM APT for 150 h followed by stepping the potential to -1200 mV for 1 h; (b) and (c) the EDX profile analyses for the area (I) and area (II) shown on the SEM image, respectively.

In order to confirm the occurrence of pitting corrosion of Mg in AGW and the ability of APT in protecting its surface, SEM and EDX investigations were carried out. Fig. 4 shows (a) SEM micrograph and (b) the corresponding EDX profile analysis for Mg surface after its immersion in AGW for 150 h followed by stepping the potential to -1200 mV for almost 1 h. The SEM image confirms the presence of a wide pit on the investigated Mg surface. The atomic percentages of the elements found inside the pit were 60.33% O, 33.29% Mg, 6.09% Cl, and 0.29% Mn. The presence of Cl indicates that the pit size can further increase with prolonging the time of the applied potential on Mg surface. The presence of low Mg content and high O percentage proves that the pit may contain $\text{Mg}(\text{OH})_2$ (reaction 3) and/or MgO [33-35];



Here, Mg first dissolved followed by the formation of Magnesium oxide and hydroxide and then attacked by Cl^- ions from AGW leading to the occurrence of pitting corrosion.

Fig. 5 shows (a) SEM micrograph and (b) and (c) the corresponding EDX spectra taken in the area (I) and area (II) seen on the SEM image, respectively for Mg surface after its immersion in AGW + 1.0 mM APT for 150 h followed by stepping the potential to -1200 mV for 1 h. The SEM image shows no pits on the whole surface but bulk corrosion products (area I) covered the majority of the surface and also some places (area II), where the corrosion products were thinner. The EDX profile analysis (Fig. 5b) for area (I) on SEM image recorded 59.09% O, 14.51% Ca, 11.66% C, 7.14% Mg, 6.42% N, 0.65% Cl, 0.28% S, 0.24% Na, and 0.00% Mn. The presence of C, N and S indicates that APT is incorporated in the formed products on the surface. This was also confirmed by the very low percentages of both Mg and Cl, also the complete absence of Mn. The atomic percentages of elements found on Mg surface in area (II, (Fig. 5c)) on SEM image were 51.50% O, 25.34% Mg, 14.89% C, 4.84% N, 2.05% Cl, 0.74% S, 0.34% Ca, and 0.31% Mn. Here, C, N and S are also present and confirm the adsorption of APT molecules onto the surface. This explains thus the decreases of the current of Mg, Fig. 3, in the presence of APT and up on the increase of its concentration.

3.3. Electrochemical impedance spectroscopy (EIS) measurements

Nyquist plots for Mg electrode at open-circuit potential after its immersion for 1 h (a) and 150 h (b) in AGS without (1) and with 1.0 mM APT (2) and 5.0 mM APT, respectively are shown in Fig. 6. These EIS measurements were performed in order to determine kinetic parameters for electron transfer reactions at the alloy/AGW interface and to confirm the data obtained by CPP and CT experiments. The impedance spectra of Fig. 6 were analysed by fitting to the equivalent circuit model shown in Fig. 7. The parameters obtained from the equivalent circuit in addition to the calculated values of IE%, are listed in Table 2. The values of IE% obtained from EIS spectra were calculated as reported before [13, 27, 31, 38]. The components of the equivalent circuit can be defined as, R_s the solution resistance between the alloy surface and the counter electrode, Q_1 and Q_2 the constant phase elements (CPEs), R_{p1} the resistance of a film layer formed on the Mg alloy surface, and R_{p2} accounts for the polarization resistance at the alloy surface.

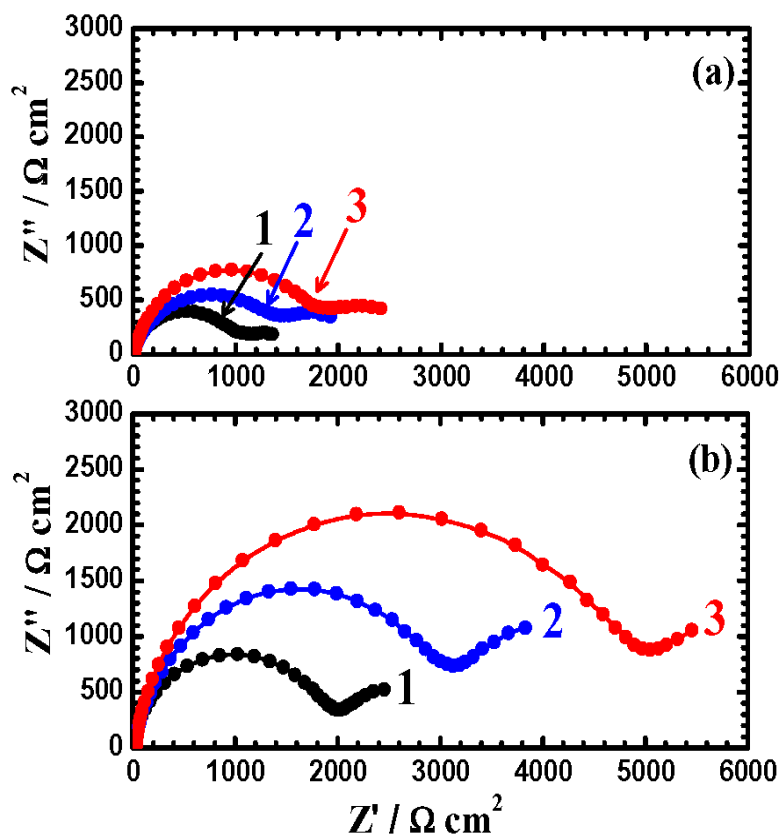


Figure 6. Nyquist plots for Mg electrode at an open-circuit potential after its immersion in the absence (1) and presence of 1.0 mM APT (2) and 5.0 mM APT for 1 h (a) and 150 h (b), respectively.

Fig. 6 and Table 2 show that increasing exposure time 150 h increased the resistance values i.e. R_S , R_{P1} and R_{P2} . The polarization resistance here ($R_P = R_{P1} + R_{P2}$) is a measure of the uniform corrosion rate as opposed to tendency towards localized corrosion.

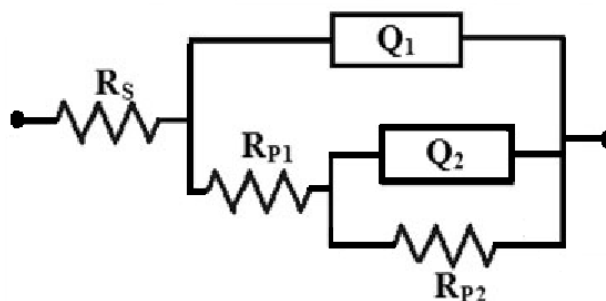


Figure 7. Equivalent circuit model used to fit the EIS experimental data presented in Fig. 6. Symbols used in the circuit are defined in the text.

This effect was significantly increased in the presence of APT and up on the increase of its concentration due to the adsorption of APT molecules on Mg surface. The CPEs, Q_1 and Q_2 with their n values close to 1.0 (especially in the presence of APT, see Table 2) represent double layer capacitors

with some pores. The CPEs decrease, while their *n*-values increase in the presence of APT. Where, the capacitive effects decrease due to the presence of APT layers with MgO and Mg(OH)₂ on the Mg alloy surface. This effect was also confirmed by the increase of the diameter of the measured EIS curves with increasing APT content and exposure time. The semicircles at high frequencies in Fig. 6 are generally associated with the relaxation of electrical double layer capacitors and the diameters of the high frequency semicircles can be considered as the charge transfer resistance (*R_p*). The EIS thus are in good agreement with those ones obtained by CPP (Fig. 2 and Table 1) and CT (Fig. 3) under the same conditions.

Table 2. EIS parameters obtained by fitting the Nyquist plots shown in Fig. 6 with the equivalent circuit shown in Fig. 7 for magnesium electrodes after 1 h and 150 h of immersion in naturally aerated AGW without and with APT.

Solution	Parameter							
	<i>R_s</i> / Ωcm ²	<i>Q</i> ₁		<i>R_{p1}</i> / Ω cm ²	<i>Q</i> ₂		<i>R_{p2}</i> / Ω cm ²	IE / %
		<i>Y</i> _{Q1} / μF cm ⁻²	<i>n</i>		<i>Y</i> _{Q2} / μF cm ⁻²	<i>n</i>		
AGW alone (1 h)	6.425	20.49	0.89	289	10.6	0.11	551	—
+ 1.0 mM APT (1 h)	12.13	0.53	1.00	940	6.97	0.79	1659	67.68
+ 5.0 mM APT (1 h)	19.02	0.47	1.00	1520	0.45	0.85	2128	76.97
AGW alone (150 h)	12.07	11.06	0.91	828	1.48	0.74	942	—
+ 1.0 mM APT (150 h)	25.89	8.68	0.87	3034	0.889	0.81	2866	70.00
+ 5.0 mM APT (150 h)	29.97	0.106	0.90	4970	0.121	0.84	3051	77.93

3. 4. Weight-loss data, SEM / EDX investigations and inhibition efficiency

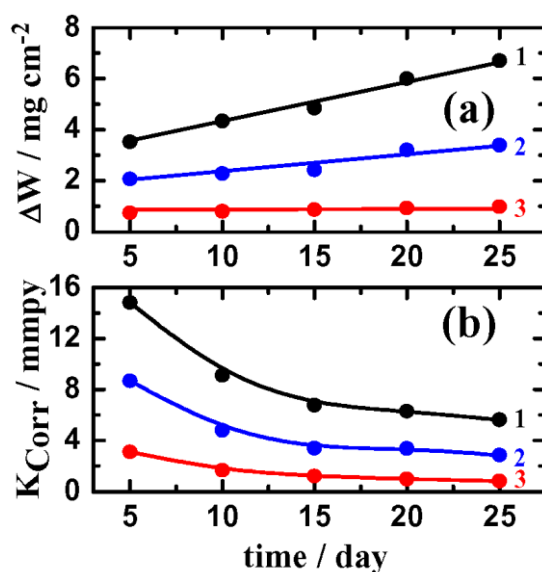


Figure 8. Variations of (a) the weight loss ($\Delta W / \text{mg} \cdot \text{cm}^{-2}$) and (b) the corrosion rate ($K_{\text{Corr}} / \text{mmpy}$) versus time for Mg coupons in naturally aerated AGW without APT (1), with 1.0 mM APT (2) and with 5.0 mM APT (3), respectively.

The variations of (a) the weight loss ($\Delta W / \text{mg.cm}^{-2}$) and (b) the corrosion rate ($K_{\text{Corr}} / \text{mmpy}$) versus time for Mg coupons in naturally aerated AGW without APT (1), with 1.0 mM APT (2) and with 5.0 mM APT (3), respectively. The values of ΔW (Fig. 8a, curve 1) increased, while the K_{Corr} (Fig. 8b, curve 1) decreased with time for Mg in AGW alone. This is due to the accumulation of corrosion products including magnesium oxide and hydroxide, which cover up the surface leading to decreasing the uniform corrosion. The presence of 1.0 mM APT (curves 2) decreased both ΔW and K_{Corr} values compared to AGW alone due to the protective action of APT molecules. More decreases were recorded for ΔW and K_{Corr} values when the concentration of APT was increased to 5.0 mM (curves 3), which is in good agreement with those ones obtained from CPP, CT and EIS we have seen earlier.

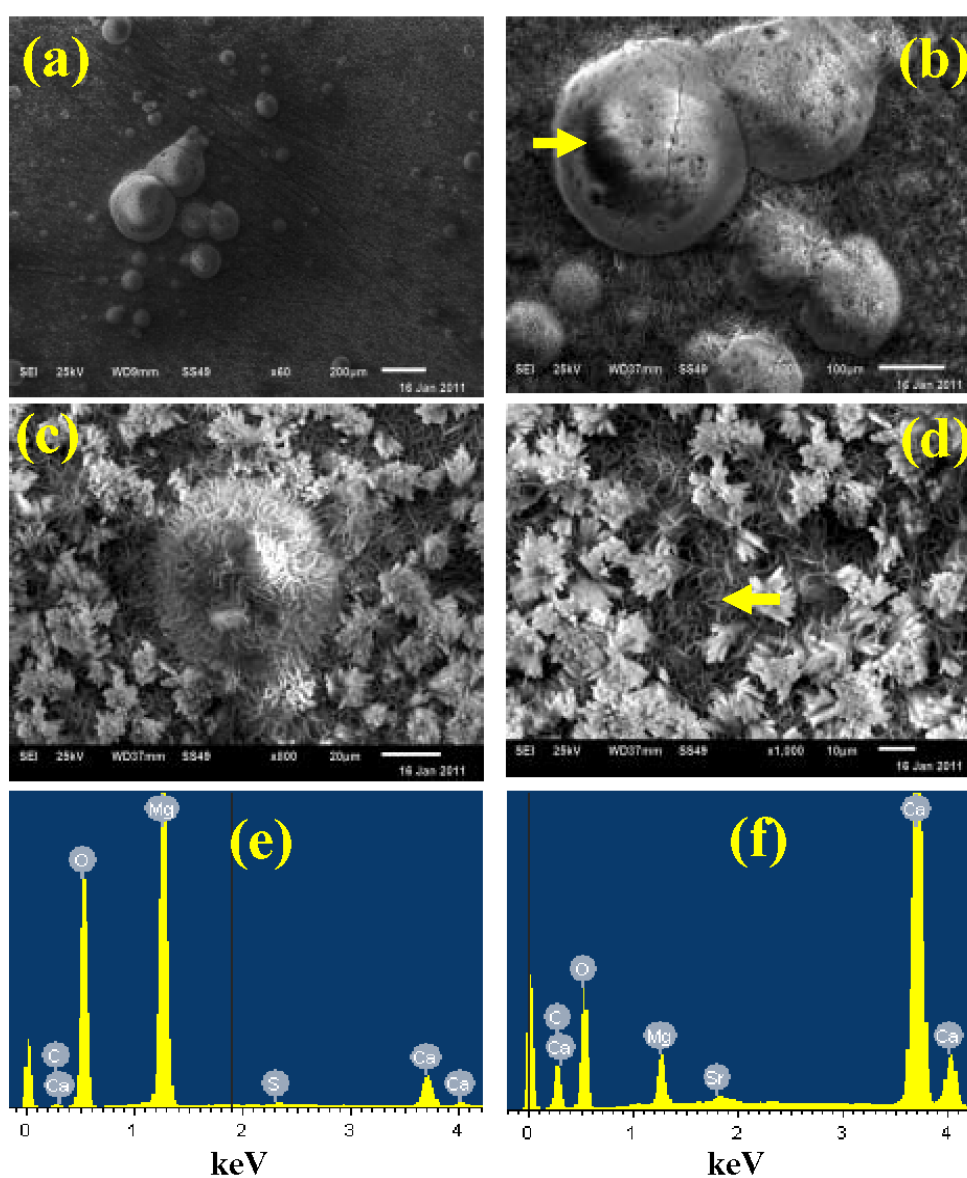


Figure 9. SEM micrographs (a), (b), (c) and (d) at different magnifications for Mg surface after its immersion in naturally aerated AGW for 25 days; EDX profile analyses (e) and (f) taken in the selected SEM areas in image (a) and (c) , respectively.

In order to differentiate between the surface morphology and to identify the composition of the species formed on the surface of the magnesium alloy after its immersion in naturally aerated AGW without and with APT, SEM/EDX investigations were carried out. Fig. 9 shows the SEM micrographs (a), (b), (c) and (d) at different magnifications for Mg surface after its immersion in naturally aerated AGW for 25 days and EDX profile analyses (e) and (f) taken in the selected SEM areas in image (b) and (d), respectively.

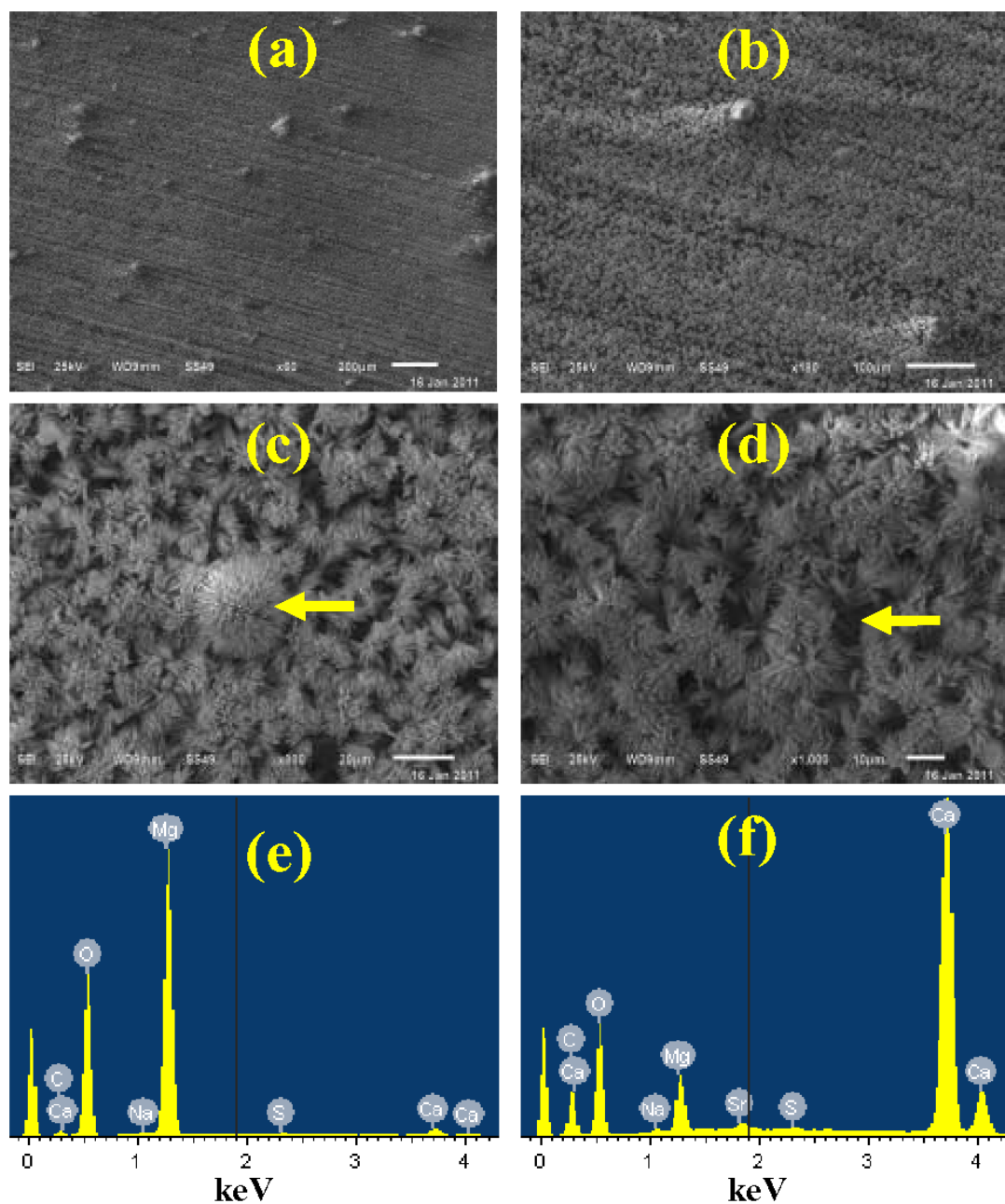


Figure 10. SEM micrographs (a), (b), (c) and (d) at different magnifications for Mg surface after its immersion in naturally aerated AGW + 1.0 mM APT for 25 days; EDX profile analyses (e) and (f) taken in the selected SEM areas in image (a) and (c), respectively.

SEM micrograph, Fig. 9a, shows that the coupons surface is fully covered with corrosion products. Increasing the magnification, Fig. 9b, indicates that the surface developed mound like corrosion products. The atomic percentages of the elements found in the selected area of SEM and displayed in the EDX profile presented in Fig. 9e, were 62.12% O, 16.11% C, 19.06% Ca, 0.14% Sr, and only 2.58% Mg with no Mn present. The minute amounts of Mg with the absence of Mn indicate that the investigated corrosion product is very thick and the compounds in this area might have formed on the coupon surface due to the presence of micro-organisms in the seawater. Further expanding the magnification of the image, Fig. 9c, shows that the surface has two areas; one is covered with grass like corrosion products from which the mounds were formed; and the other area is covered with thinner corrosion products. That is clear in Fig. 9d, where the magnification is the highest. The EDX spectrum for the selected area of Fig. 9d is shown in Fig. 9f. The atomic percentages of elements found in this area were, 66.70% O, 26.84% Mg, 3.99% C, 2.32% Ca, and 0.15% S.

Fig. 10 shows the SEM micrographs (a), (b), (c) and (d) with increased magnifications for Mg surface after its immersion in naturally aerated AGW + 1.0 mM APT for 25 days and EDX profile analyses (e) and (f) taken in the selected areas in SEM images (a) and (c), respectively. The SEM images show that the surface of Mg is covered with a thick homogenous film of corrosion products. Increasing the SEM magnification indicates that the surface has grass like corrosion products area and another smaller area is different in its appearance. The atomic percentages found in the developed grass like area, Fig. 10c, recorded 61.24% O, 27.00% Mg, 10.66% C, 0.73% Ca, 0.20% S and 0.18% Na. On the other hand, the EDX analysis (Fig. 10f) for the selected SEM area that is shown in Fig. 10d, 60.58% O, 18.80% C, 17.20% Ca, 3.12% Mg, 0.16% Sr, 0.12% S and 0.2% Na. The very low content of Mg and the absence of Mn indicate that the alloy surface is completely covered with a thick layer of corrosion products.

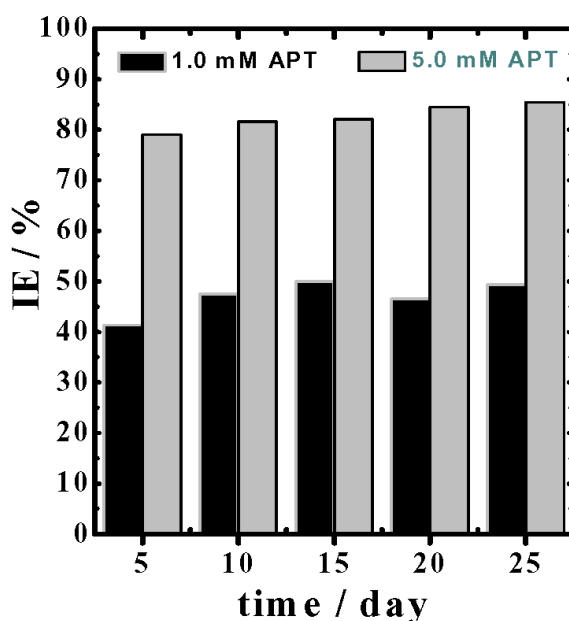


Figure 11. Variations of the inhibition efficiency ($IE\%$) versus time for Mg coupons in naturally aerated AGW by 1.0 mM APT and 5.0 mM APT, respectively.

The change of the inhibition efficiency ($IE\%$) calculated from weight-loss with time for Mg coupons in AGW by 1.0 and 5.0 mM APT, respectively is shown in Fig. 11. It is seen from Fig. 11 that 1.0 mM APT recorded about 42% after 5 days and reached circa 51% in 25 days. These values increased in the presence of 5.0 mM APT to 80% and 86%, respectively. This indicates that APT molecules have the ability to protect the Mg surface in AGW and its efficiency as a corrosion inhibitor increases with the increase of its concentration as well as the increase of the exposure time of the alloy in the test solution.

4. CONCLUSIONS

The corrosion and corrosion inhibition of Mg–Mn alloy after different exposure intervals in naturally aerated Arabian Gulf water (AGW) by 5-(3-aminophenyl)-tetrazole (APT) were reported. Conventional electrochemical, impedance, gravimetric, SEM and EDX investigations were used. Cyclic polarization, current-time and impedance spectroscopy measurements for Mg in AGW revealed that increasing exposure time decreases the uniform corrosion and increases pitting attack of the alloy. These measurements indicated also that the presence of APT and the increase of its concentration significantly decrease both of the corrosion forms. Weight-loss data confirmed the obtained results by polarization, current-time and impedance. SEM micrographs and EDX investigations after different experimental conditions for alloy coupons in AGW with and without APT showed that the alloy may suffer microbial induced corrosion in addition to uniform and pitting attacks; this effect decreases in the presence of APT and the increase of its concentration. Results collectively are internally consistent with each other, showing that Mg–Mn alloy highly corrodes in AGW and APT molecules preclude the corrosion of Mg through their adsorption onto the surface.

ACKNOWLEDGMENT

This project was supported by King Saud University, Deanship of Scientific Research, College of Engineering Research Center.

References

1. K.U. Kainer, F. Kaiser, Eds. *Magnesium alloys and technology*, Weinheim Verlag GmbH & Co. KG aA Wiley-VCH GmbH (2003).
2. M.M. Avedesian, H. Baker, Eds. *Magnesium and magnesium alloys*, Materials Park, OH, ASM International (1999).
3. Sebastián Feliu Jr., C. Maffiotte, Alejandro Samaniego, Juan Carlos Galván, Violeta Barranco, *Electrochim. Acta*, 56 (2011) 4554.
4. M. Hakamada, T. Furuta, Y. Chino, Y. Q. Chen, H. Kusuda, M. Mabuchi, *Energy*, 32 (2007) 1352.
5. Andrej Atrens, Nicholas Winzer, Wolfgang Dietzel, *Adv. Eng. Mater.*, 13 (2011) 11.
6. U.C. Nwaogu, C. Blawert, N. Scharnagl, W. Dietzel, K.U. Kainer, *Corros. Sci.*, 52 (2010) 2143.
7. Guangling Song, Andrej Atrens, *Adv. Eng. Mater.*, 5 (2003) 837.
8. Anna Da Forno, Massimiliano Bestetti, *Adv. Mater. Res.*, 138 (2010) 79.
9. S. Yu. Kondrat'ev, G. Ya. Yaroslavskii, B.S. Chaikovskii, *Strength Mater.*, 18 (1986) 1325.

10. S.M.M. Shanab, M.A. Ameer, A.M. Fekry, A.A. Ghoneim, E.A. Shalaby, *Int. J. Electrochem. Sci.*, 6 (2011) 3017.
11. J. Kim, K. C. Wong, P. C. Wong, S. A. Kulinich, J. B. Metson, K. A. R. Mitchell, *Appl. Surf. Sci.*, 253 (2007) 4197.
12. A.R. Shashikala, R. Umarani, S.M. Mayanna, A.K. Sharma, *Int. J. Electrochem. Sci.*, 3 (2008) 993.
13. E.M. Sherif, S.-M. Park, *Corros. Sci.*, 48 (2006) 4065.
14. E.-S. M. Sherif, A.A. Almajid, *J. Appl. Electrochem.*, 40 (2010) 1555.
15. E.-S. M. Sherif, *Int. J. Electrochem. Sci.*, 6 (2011) 1479.
16. E.-S. M. Sherif, A.H. Ahmed, *Synthesis and Reactivity in Inorganic, Metal-Organic, and Nano-Metal Chemistry*, 40 (2010) 365.
17. E.-S. M. Sherif, R. M. Erasmus, J. D. Comins, *Electrochim. Acta*, 55 (2010) 3657.
18. E.-S. M. Sherif, *J. Mater. Eng. Perform.*, 19 (2010) 873.
19. E.-S. M. Sherif, R.M. Erasmus, J.D. Comins, *Corros. Sci.*, 50 (2008) 3439.
20. G. Song, D.H. StJohn, *Mater. Corros.*, 56 (2005) 15.
21. E.-S. M. Sherif, R. M. Erasmus, J. D. Comins, *J. Colloid. Inter. Sci*, 311 (2007) 144.
22. Adel Mesbah, Caroline Juers, Françoise Lacouture, Stéphane Mathieu, Emmanuel Rocca, Michel François, Jean Steinmetz, *Solid State Sci.*, 9 (2007) 322.
23. Xu Yang, Fu Sheng Pan, Ding Fei Zhang, *Materials Science Forum*, 610–613 (2009) 920.
24. E.-S. M. Sherif, R.M. Erasmus, J.D. Comins, *J. Appl. Electrochem.*, 39 (2009) 83.
25. E.-S. M. Sherif, *Mater. Chem. Phys.*, 129 (2011) 961.
26. E.-S. M. Sherif, A.A. Almajid, *Int. J. Electrochem. Sci.*, 6 (2011) 2131.
27. E.M. Sherif, S.-M. Park, *Electrochim. Acta*, 51 (2006) 6556.
28. E.-S. M. Sherif, A.A. Almajid, F.H. Latif, H. Junaedi, *Int. J. Electrochem. Sci.*, 6 (2011) 1085.
29. E.-S. M. Sherif, J.H. Potgieter, J.D. Comins, L. Cornish, P.A. Olubambi, C.N. Machio, *Corros. Sci.*, 51 (2009) 1364.
30. E.-S. M. Sherif, J.H. Potgieter, J.D. Comins, L. Cornish, P.A. Olubambi, C.N. Machio, *J. Appl. Electrochem.*, 39 (2009) 1385.
31. E.M. Sherif, S.-M. Park, *Electrochim. Acta*, 51 (2006) 4665.
32. E.-S. M. Sherif, *Int. J. Electrochem. Sci.*, 6 (2011) 2284.
33. Zhiming Shi, Andrej Atrens, *Corros. Sci.*, 53 (2011) 226.
34. A.Pardo, M.C. Merino, A.E. Coy, R. Arrabal, F. Viejo, E. Matykina, *Corros. Sci.*, 50 (2008) 823.
35. S. Bender, J. Goellner, A. Heyn, E. Boese, *Mater. Corros.*, 58 (2007) 977.
36. A.A. El Warraky, H.A. El Shayeb, E.M. Sherif, *Anti-Corros. Methods Mater.*, 51 (2004) 52.
37. Z. Szklarska-Smialowska, editor. *Pitting Corrosion of Metals*, Nace International, Houston (1986).
38. E.-S. M. Sherif, *Int. J. Electrochem. Sci.*, 6 (2011) 3077.